

# Lag-modeling approach for dissipation terms in large eddy simulation

By S. G. Chumakov, J. Larsson, C. Schmitt AND H. Pitsch

## 1. Motivation and objective

In Large Eddy Simulation (LES), only the large energy-containing scales of motions are computed directly, while the effect of the small scales is accounted for via the subgrid-scale (SGS) models. The governing equations for LES are obtained by formally applying the filtering procedure  $\bar{\phi} = G * \phi$  to the Navier-Stokes equations:

$$\bar{u}_{i,i} = 0 \quad (1.1)$$

$$\bar{u}_{i,t} + (\bar{u}_i \bar{u}_j)_{,j} = -\bar{P}_{,i} + \nu \bar{u}_{i,jj} - \tau_{ij,j}. \quad (1.2)$$

Here  $*$  denotes convolution,  $\tau_{ij} = \overline{u_i u_j} - \bar{u}_i \bar{u}_j$  is the SGS stress tensor,  $G$  is the filter function that satisfies  $\|G\|_1 = 1$ ,  $G \geq 0$ ,  $\nu$  is the kinematic viscosity, and  $P = p/\rho$  is the modified pressure. The following notations are used to designate the derivatives:  $a_{,i} = \partial a / \partial x_i$ ,  $a_{,ij} = \partial^2 a / \partial x_i \partial x_j$ , and  $a_{,t} = \partial a / \partial t$ .

Applying similar averaging to the transport equation for a passive scalar  $\phi$  yields

$$\bar{\phi}_{,t} + (\bar{u}_i \bar{\phi})_{,i} = D \bar{\phi}_{,ii} - h_{i,i}. \quad (1.3)$$

Here  $h_i = \overline{u_i \phi} - \bar{u}_i \bar{\phi}$  is the SGS scalar flux. Both  $\tau_{ij}$  and  $h_i$  are not available from the resolved (LES) flow field and thus have to be modeled.

A very promising approach to modeling  $\tau_{ij}$  and  $h_i$  consists of utilization of extra LES quantities such as SGS kinetic energy (Schumann 1975; Ghosal *et al.* 1995) and SGS scalar variance (Jiménez *et al.* 2001; Chumakov & Rutland 2004, 2005). For these quantities, transport equations can be rigorously derived:

$$k_{s,t} + (\bar{u}_i k_s)_{,i} = -(\overline{u_i P_{,i}} - \bar{u}_i \bar{P}_{,i}) - (\tau_{ij,j} / 2 - \bar{u}_i \tau_{ij})_{,j} + \nu k_{s,jj} - \tau_{ij} \bar{S}_{ij} - \epsilon_s \quad (1.4)$$

$$\theta_{,t} + (\bar{u}_i \theta)_{,i} = -(\overline{u_i \phi^2} - \bar{u}_i \bar{\phi}^2)_{,i} + 2\bar{\phi} h_{i,i} + D \theta_{,ii} - \chi_s. \quad (1.5)$$

Here  $k_s = \tau_{ii} / 2$  is the SGS energy,  $\tau_{ij} = \overline{u_i u_j u_j} - \bar{u}_i \bar{u}_i \bar{u}_j$  is the triple-correlation term, and  $\bar{S}_{ij} = (\bar{u}_{i,j} + \bar{u}_{j,i}) / 2$  is the resolved strain-rate tensor. In the second equation,  $\theta = \overline{\phi^2} - \bar{\phi}^2$  is the SGS scalar variance.

The customary treatment of the equations (1.4) and (1.5) consists of modeling the triple-correlation terms with turbulent viscosity  $\nu_T$  or turbulent diffusivity  $D_T$ . The second term on the right-hand side of (1.5) is recast as  $2\bar{\phi} h_{i,i} = (2\bar{\phi} h_i)_{,i} - 2h_i \bar{\phi}_{,i}$  and the first part of it, together with the triple correlation term is modeled via turbulent diffusivity  $D_T$ . This simplifies the equations for  $k_s$  and  $\theta$  to the following:

$$k_{s,t} + (\bar{u}_i k_s)_{,i} = (\nu + \nu_T) k_{s,jj} \underbrace{- \tau_{ij} \bar{S}_{ij}}_{\Pi} - \epsilon_s \quad (1.6)$$

$$\theta_{,t} + (\bar{u}_i \theta)_{,i} = (D + D_T) \theta_{,ii} \underbrace{- 2h_i \bar{\phi}_{,i}}_{\Lambda} - \chi_s, \quad (1.7)$$

where  $\Pi$  and  $\Lambda$  are the source terms for  $k_s$  and  $\theta$ , correspondingly.

The simplified equations have new unclosed terms:

$$\epsilon_s = \nu (\overline{u_{i,j} u_{i,j}} - \bar{u}_{i,j} \bar{u}_{i,j}) \quad (1.8)$$

the SGS energy dissipation rate, and the dissipation rate of the SGS scalar variance

$$\chi_s = 2D (\overline{\phi_{,i} \phi_{,i}} - \bar{\phi}_{,i} \bar{\phi}_{,i}). \quad (1.9)$$

Both of these terms have to be modeled. The latter term,  $\chi_s$ , also plays an important role in combustion modeling, e.g., in the flamelet models for non-premixed combustion (for review, see Pitsch 2006).

In the current literature, few models can be found for  $\epsilon_s$  and  $\chi_s$ . For  $\epsilon_s$ , the standard model is (Schumann 1975; Yoshizawa & Horiuti 1985)

$$\epsilon_s \approx 1.0 \frac{k_s^{3/2}}{\Delta}, \quad (1.10)$$

where  $\Delta$  is the characteristic length scale of the LES filter (usually  $\Delta$  is set to the LES grid cell size). This model has been found to over-predict the actual dissipation rate in a priori tests by Chumakov (2007). Therefore application of this model in conjunction with the eddy-viscosity models for  $\tau_{ij}$  results in stable calculations owing to forward-only energy transfer between resolved and subgrid scales and local equilibrium assumption applied to the subgrid scales.

Modeling of  $\chi_s$ , along with modeling for  $\theta$ , has been an active research area due to demand from the combustion community. Pierce & Moin (1998) applied the dynamic procedure to modeling  $\theta$  and  $\chi_s$  as  $\theta \approx C \Delta^2 \bar{\phi}_{,i} \bar{\phi}_{,i}$  and  $\chi_s = (D + D_T) \bar{\phi}_{,i} \bar{\phi}_{,i}$ . Cook & Bushe (1999) proposed to use the assumed scalar spectrum to compute the coefficient  $C$  in the model for  $\chi_s$ . Recent advances include application of the concept of optimal estimators (Balarac *et al.* 2008*a,b*) to model both terms. Also, various numerical issues that complicate the modeling of  $\theta$  have been considered in Kaul *et al.* (2009). In particular, under some circumstances it was found to be preferable to use the transport equation for  $\overline{\phi^2}$  in place of the transport equation for  $\theta$ . Although we do not investigate the effect of numerical implementation here, these ideas can be applied in further development of the concepts presented in this work. In general, one should always take into account the numerical errors that can be of considerable magnitude in LES (Ghosal 1999). A further comprehensive review of closures for  $\theta$  and  $\chi_s$  can be found in Pitsch (2006).

All models mentioned above relate the dissipation terms to other (known) quantities at the same instant in time and, as a rule, imply that the subgrid flow is in local equilibrium, i.e., production and dissipation of SGS energy (or SGS scalar variance) are equal. The latter assumption is clearly violated in some important cases (Pitsch 2006), whereas the former can be generalized as follows: we can relate the dissipation at time  $t_0$  to other quantities over a time interval  $(t_0 - T, t_0)$  instead of a single snapshot of the flow at  $t = t_0$ . For example, one phenomenological picture could be that there is a time-lag between the transfer of energy into the subgrid scales and the dissipation into heat of an imagined energy packet. In the present work we construct models that introduce a time-lag into the process, and investigate whether this leads to better predictions.

In summary, the dissipation field  $\chi_s$  at the moment  $t = t_0$  might not be correlated with the resolved field at  $t = t_0$ , but there is a possibility of correlation between  $\chi_s$  and the resolved field at the time  $t = t_0 - T$ , where  $T$  is some characteristic lag time. A simple idea inspired in part by Lagrangian approach to the modeling of  $\tau_{ij}$  (Meneveau

*et al.* 1996) is to model the dissipation terms as the production terms, lagged along the Lagrangian trajectories. To evaluate the feasibility of this approach is the main objective of this work.

## 2. Formulation of the modeling approach

### 2.1. *A priori verification of modeling assumption*

Before we start model derivation, we should determine if the main assumption, i.e., that the dissipation is lagging behind the production along a Lagrangian trajectory, is valid. For this we use direct numerical simulation (DNS) of forced isotropic turbulence with LES Lagrangian particles.

An open-source, pseudo-spectral code `hit3d†`, developed by one of the authors, has been used for the a priori testing of the modeling assumptions. The main purpose of the code is to perform large-scale DNS of incompressible homogeneous isotropic turbulence with an arbitrary number of passive scalars in a massively parallel environment. Also, the code is capable of transporting Lagrangian particles that are advected by locally averaged flow field to mimic the particles carried by "ideal" LES. The characteristic length  $\Delta$  of the LES filter can be varied and various quantities can be computed along the particle trajectories.

For the purposes of this work, we ran a DNS of forced isotropic turbulence with  $Re_\lambda = 230$ . The size of the computational domain was  $512^3$  grid points. The LES filter length  $\Delta$  was set to 0.2 and 0.4, which falls into the (although limited) inertial range of the simulation. We measured  $\Pi$ ,  $\Lambda$ ,  $\epsilon_s$ , and  $\chi_s$  along the LES particle trajectories and computed the cross-correlation between  $\Pi(t)$  and  $\epsilon_s(t+T)$ . The resulting correlation was averaged over 100,000 particle trajectories and is presented in the Fig. 1. It is evident from the figure that there is a noticeable lag between the production and dissipation of SGS energy, and the lag time equals roughly one eddy turnover time at the cutoff scale. The eddy turnover time is calculated as  $1/|\bar{S}|$ . Similar results have been obtained for  $\Lambda$  and  $\chi_s$  (not shown).

Thus our a priori test shows that there is indeed lag between production and dissipation. Now we can build our model on this assumption.

### 2.2. *Model derivation*

The cornerstone of our approach is the concept of cascade time scale, which we will illustrate using the SGS energy dissipation rate  $\epsilon_s$  as an example. Model derivation for  $\chi_s$  is identical.

We surmise that once energy (or scalar variance) is injected in a ball of fluid of radius  $\Delta$ , where  $\Delta$  is in the inertial range of scales, it is carried by the eddies with the characteristic size of the order of  $\Delta$ . Then the eddy breakdown process carries this energy into smaller and smaller scales until it reaches dissipative scales of motion and dissipates. The duration of this process is characterized by the cascade timescale. We assume that the ball retains its shape during this time. This process results in the lag between production of the SGS energy at the scales similar to  $\Delta$ , the LES filter size, and its dissipation at the scales of the order of  $\eta$ , the Kolmogorov length scale.

Thus the dissipation rate  $\epsilon_s$  can be found as an integral of the production rate  $\Pi = -\tau_{ij}\bar{S}_{ij}$  along the LES Lagrangian trajectory with a particular weight function that has

† The code is freely available from [hit3d.googlecode.com](https://github.com/hit3d)

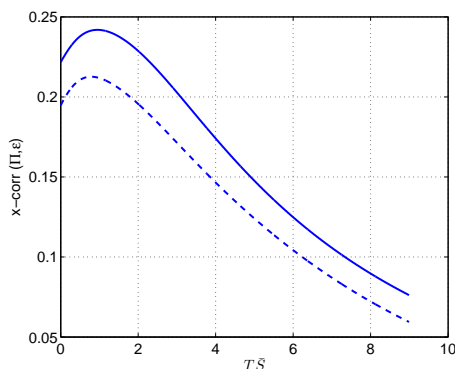


FIGURE 1. The cross-correlation between production  $\Pi$  and dissipation  $\epsilon_s$  of the SGS energy  $k_s$  along LES Lagrangian trajectories with  $\Delta = 0.2$  (—) and  $\Delta = 0.4$  (----). The time shift  $T$  is normalized by the eddy timescale  $1/\bar{S}$ .

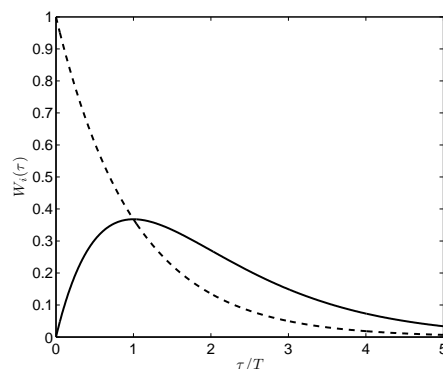


FIGURE 2. Weight functions  $W_0$  (----) and  $W_1$  (—).

the peak at some characteristic time  $T$ . We introduce the weight functions  $W_0(x)$  and  $W_1(x)$  defined as follows (see Figure 2):

$$W_0(x) = \exp(-x/T), \quad W_1(x) = \frac{x}{T} \exp(-x/T). \quad (2.1)$$

These functions possess the following property:

$$\frac{\partial}{\partial t} W_1(t-t') = \frac{1}{T} [W_0(t-t') - W_1(t-t')]. \quad (2.2)$$

Thus we can rewrite  $\epsilon_s$  as the Lagrangian average of  $\Pi$  with the weight  $W_1$ . We introduce an auxiliary quantity  $B$  as the similar average of  $\Pi$  but with the weight function  $W_0$  as follows:

$$(BT)(t, x(t)) = \int_{-\infty}^t \Pi(t', x(t')) W_0(t-t') dt', \quad (2.3)$$

$$(\epsilon_s T)(t, x(t)) = \int_{-\infty}^t \Pi(t', x(t')) W_1(t-t') dt'. \quad (2.4)$$

Taking derivatives of both sides in the equations (2.3) and (2.4) and using the property (2.2), we arrive at the following ODE system:

$$\begin{cases} (\dot{BT}) &= \Pi - B \\ (\dot{\epsilon}_s T) &= B - \epsilon_s \end{cases}, \quad (2.5)$$

where the derivatives are taken along the Lagrangian path. Note that the system conserves the energy, i.e., the long-term averages of  $\Pi$  and  $\epsilon_s$  along the Lagrangian path are equal.

The system (2.5) has been tested a priori with two kinds of parameter function  $\Pi$ : synthetic (Gaussian random) and  $\Pi$  taken from a DNS, and was found to have several potential problems. Namely, (i) in this particular formulation of the system nothing prevents  $\epsilon_s$  from going negative which is unphysical, and (ii) the system does not take

into account the turbulent diffusion of the SGS energy. The point (i) can be taken care of by introducing separate timescales for  $B$  and  $\epsilon_s$ .

$$\begin{cases} (B\dot{T}_B) &= \Pi - B \\ (\epsilon_s\dot{T}_\epsilon) &= B - \epsilon_s \end{cases}, \quad (2.6)$$

The timescales are further defined as  $T_B = 1/|\bar{S}|$ ,  $T_\epsilon = C_T\Delta^{2/3}\epsilon_s^{-1/3}$ . The latter prevents  $\epsilon_s$  from going negative. We assume that these timescales are close in the situation of fully developed turbulent flow, i.e., when both  $k_s$  and  $\epsilon_s$  are nonzero. The phase portraits of the system (2.6) in the  $(B, \epsilon_s)$ -plane are given in the Figures 3, 4 and 5. The system has a fixed point at  $(\Pi, \Pi)$  for all values of  $\Pi$ , but the trajectories always stay in the upper half-plane,  $\epsilon_s \geq 0$ , independent of  $\Pi$ , if the initial conditions satisfy  $\epsilon_s \geq 0$ . Also for constant zero  $\Pi$  the dissipation rate converges to zero.

To rectify the point (ii) mentioned above, we need to replace the left-hand side of (2.6) with material derivative and add the turbulent diffusion to the right-hand side of the system. This changes the system (2.6) as follows:

$$\begin{cases} (BT_B)_{,t} + (\bar{u}_i BT_B)_{,i} &= (\nu + \nu_T)(BT_B)_{,ii} + \Pi - B \\ (\epsilon_s T_\epsilon)_{,t} + (\bar{u}_i \epsilon_s T_\epsilon)_{,i} &= (\nu + \nu_T)(\epsilon_s T_\epsilon)_{,ii} + B - \epsilon_s \end{cases}. \quad (2.7)$$

The system (2.7) still has the conservation property, i.e., the net production equals net dissipation over long time periods. Moreover, with this model for  $\epsilon_s$ , the transport equation for  $k_s$  (1.6), becomes redundant, because it is equivalent to the sum of the equations that comprise the system (2.7); thus,  $k_s = (BT_B) + (\epsilon_s T_\epsilon)$ .

Alternatively, one could view the equation for  $(BT_B)$  as redundant and solve for  $k_s$  and  $\epsilon_s T_\epsilon$  with  $B = (k_s - \epsilon_s T_\epsilon)/T_B$ . Thus one would obtain a two-equation model similar to the classical  $k$ - $\epsilon$  model. The differences compared with the classical model are (i) the lag-model solves for  $\epsilon_s T_\epsilon$  rather than  $\epsilon_s$ , and (ii) the source terms in the lag-model stem directly from the basic assumption of the form of the Lagrangian lag. This model formulation will be explored in the immediate future.

Equivalent analysis can be performed for the modeling of  $\chi_s$ . For this case, the resulting system of equations is

$$\begin{cases} (FT_F)_{,t} + (\bar{u}_i FT_F)_{,i} &= (D + D_T)(FT_F)_{,ii} + \Lambda - F \\ (\chi_s T_\chi)_{,t} + (\bar{u}_i \chi_s T_\chi)_{,i} &= (D + D_T)(\chi_s T_\chi)_{,ii} + F - \chi_s \end{cases} \quad (2.8)$$

Analogously, this system makes the equation (1.7) redundant because  $\theta = (FT_F) + (\chi_s T_\chi)$ .

### 3. A posteriori tests and results

#### 3.1. The Sydney bluff body flame

The SMH1-flame from a series of bluff body/swirl-stabilized flame experiments is used to analyze the effect of the lag-model for the SGS dissipation rate  $\chi_s$  of the variance of a passive scalar in a turbulent reactive flame simulation. Subgrid scalar dissipation rate appears here naturally in the transport equation for  $\theta$ , the SGS variance of the mixture fraction  $Z$ .

The burner configuration of this well-characterized flame consists of a central fuel nozzle of 3.6 mm diameter that is surrounded by a bluff body with  $D_{ref} = 50$  mm diameter. Swirling air at an axial bulk velocity of  $U_s = 42.8$  m/s is supplied through

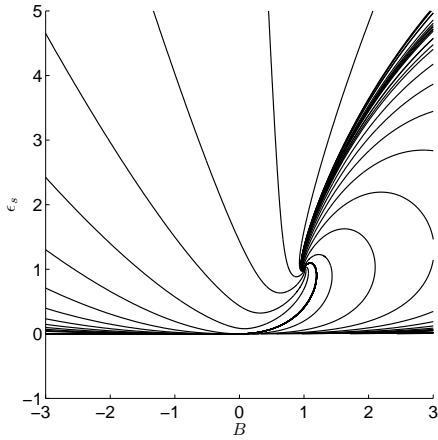


FIGURE 3. Phase portrait of the system (2.6) for the case  $\Pi = 1$ .

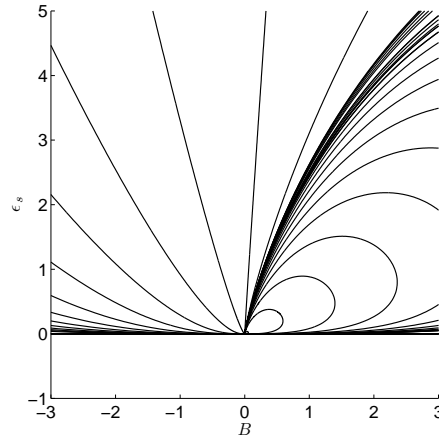


FIGURE 4. Phase portrait of the system (2.6) for the case  $\Pi = 0$ .

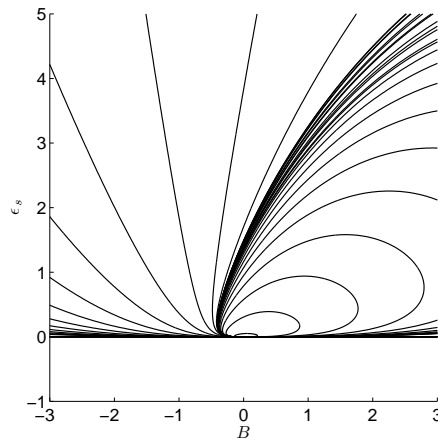


FIGURE 5. Phase portrait of the system (2.6) for the case  $\Pi = -1$ .

an annulus of 10 mm width. The burner is surrounded by a co-flowing air stream with an axial velocity of  $U_e = 20$  m/s. The fuel consists of a methane/hydrogen mixture in a volumetric ratio of 1:1. The bulk exit velocity of the fuel stream is  $U_j = 140.8$  m/s. The geometric swirl number for this configuration is  $S_g = 0.32$ . The turbulent flow field of this flame series was measured by Kalt *et al.* (2002); Al-Abdeli & Masri (2003); Masri *et al.* (2004), species measurements were performed by Kalt *et al.* (2002); Masri *et al.* (2004), and all experimental results are available online from Masri (2006).

The Favre-filtered transport equations for mass, momentum, mixture fraction, and residual mixture fraction variance are solved in cylindrical coordinates using the NGA code developed at CTR (for code reference see Desjardins *et al.* 2008). The computational domain is  $5D_{ref} \times 3D_{ref} \times 2\pi$  in axial, radial, and circumferential directions, respectively. The radial direction is discretized by 230 unevenly spaced grid points concentrated in the

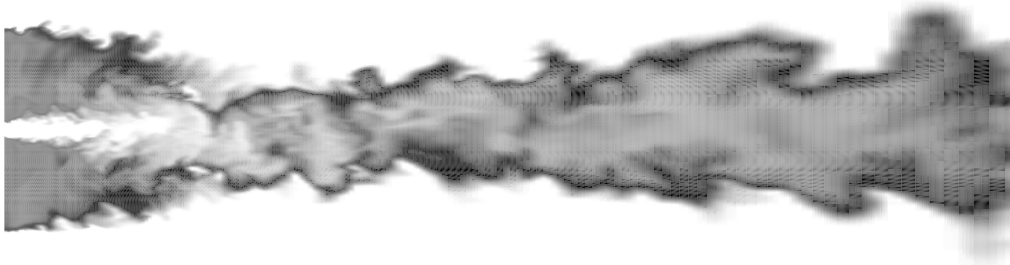


FIGURE 6. Instantaneous plot of the temperature field for the SMH1 flame. Temperature ranges from 300K (white) to 2100K (black).

shear layer region surrounding the fuel jet and swirling annulus. The grid in axial direction uses 216 points and is stretched in downstream direction whereas the circumferential direction is equally spaced and uses 64 points. The turbulent inflow profiles for the fuel nozzle and annulus are computed from a separate pipe flow simulation by enforcing the bulk axial and azimuthal velocity reported in the experiment.

The GRI 2.11 mechanism (Bowman *et al.* 1997) is used for the description of chemistry and a mapping of all relevant quantities onto the mean of mixture fraction, its variance, and scalar dissipation rate is used following the flamelet-based modeling approach proposed by Peters (1983, 1984). Due to the swirling co-flow in this configuration, the flame burns very stably and does not show strong extinction or re-ignition. There is, however, expected to be a rather strong effect of heat transfer to the bluff body, which at this point is not taken into consideration when modeling chemistry.

Figure 6 shows a snapshot of the instantaneous temperature field, which clearly shows that the flame is almost attached to the edge of the bluff body. The surrounding swirling air leads to a contraction of the flame with its neck located roughly one bluff body diameter downstream. The neck region is expected to have high dissipation rates due to presence of high gradients of both velocity and scalars, and the effect of the model for  $\chi_s$  is expected to be most prominent near that region.

The values of  $\chi_s$  and  $\bar{\chi}$  — the SGS dissipation of  $\theta$  and the full scalar dissipation which is processed by the combustion model, — are presented in Figure 7. Same values, but conditioned on the resolved mixture fraction  $\tilde{Z}$ , are plotted in Figure 8. The statistical results for temperature and mass fraction of  $\text{CO}_2$  for the two simulations are reported in Figure 9 with comparison to experimental data.

As mentioned above, it is not surprising to find a clear discrepancy between simulations and experiment close to the bluff body. At the first station the heat transfer to the bluff body seems to have a large effect, but it is not taken into account in the simulation setup. At the last two stations the statistics are strongly affected by how well the swirling co-

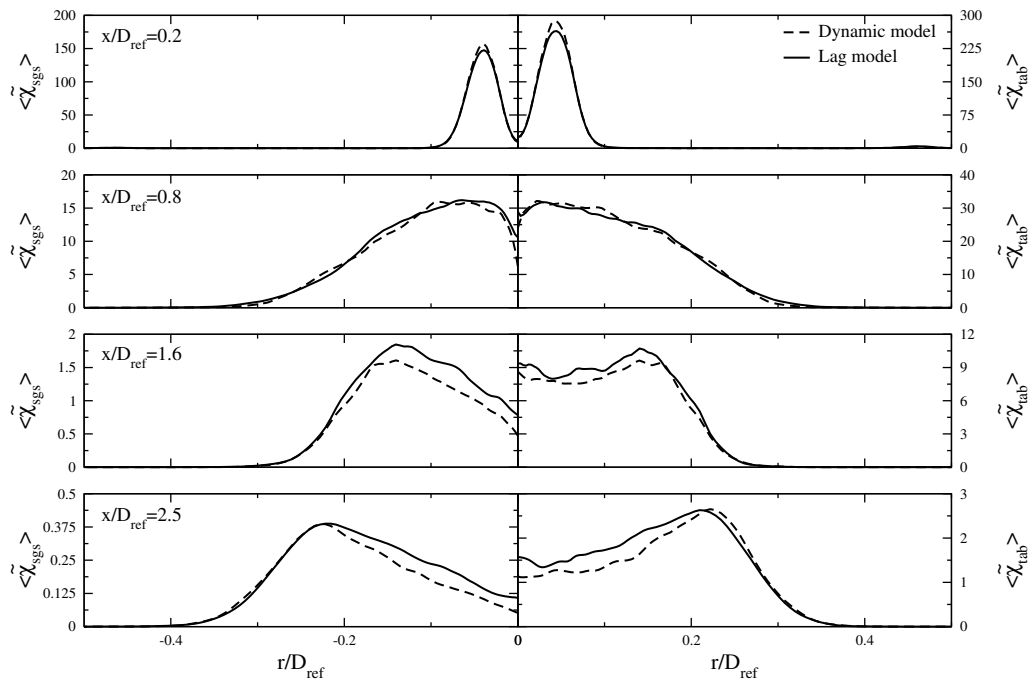


FIGURE 7. Statistics of the mean of the SGS scalar dissipation  $\chi_s$  and full scalar dissipation  $\bar{\chi}$  recovered from the simulation, at four downstream locations,  $x/D_{ref} = 0.2, 0.8, 1.6, 2.5$  (from top to bottom). The simulation based on a standard dynamic procedure to evaluate the subgrid scalar dissipation rate is shown by the dashed line, and the simulation based on the lag-model corresponds to the solid line.

flow is captured, and therefore are not suited for detailed study of lagged versus standard models of the scalar dissipation.

It is evident from the Figures that near the neck region of the flame (at the second measuring station) the time-averaged values of both  $\chi_s$  and  $\bar{\chi}$  do not change dramatically (Figure 7). However, there is a difference between the conditioned values (Figure 8). The peaks at the right end of the graphs of  $\langle \chi_s | \tilde{Z} \rangle$  and  $\langle \bar{\chi} | \tilde{Z} \rangle$ , which are absent in the simulation with the dynamic model, may indicate the further penetration of the fuel jet inside the domain in the simulation with the lag-model. For lower values of  $\tilde{Z}$ , the difference between the predictions of the dynamic and lag-model is also apparent. The effect of the lag-model on the resolved statistics is shown in the Figure 9. Here, a clear difference in prediction of the temperature and, consequently, reaction products, can be seen at the second measuring station. The simulation with lag-model gives predictions of Favre-averaged temperature  $\tilde{T}$  and the mass fraction of  $\text{CO}_2$  that are closer to the ones measured experimentally. As a result of changing only one variable in the whole simulation, we consider this an improvement.

#### 4. Summary and future work

A new approach to modeling the dissipation of subgrid-scale energy and subgrid-scale scalar variance in the framework of Large Eddy Simulation is introduced. The approach is based on the idea of incorporating an explicit delay (or lag) between the production and dissipation terms in the transport equations for the SGS energy and SGS scalar

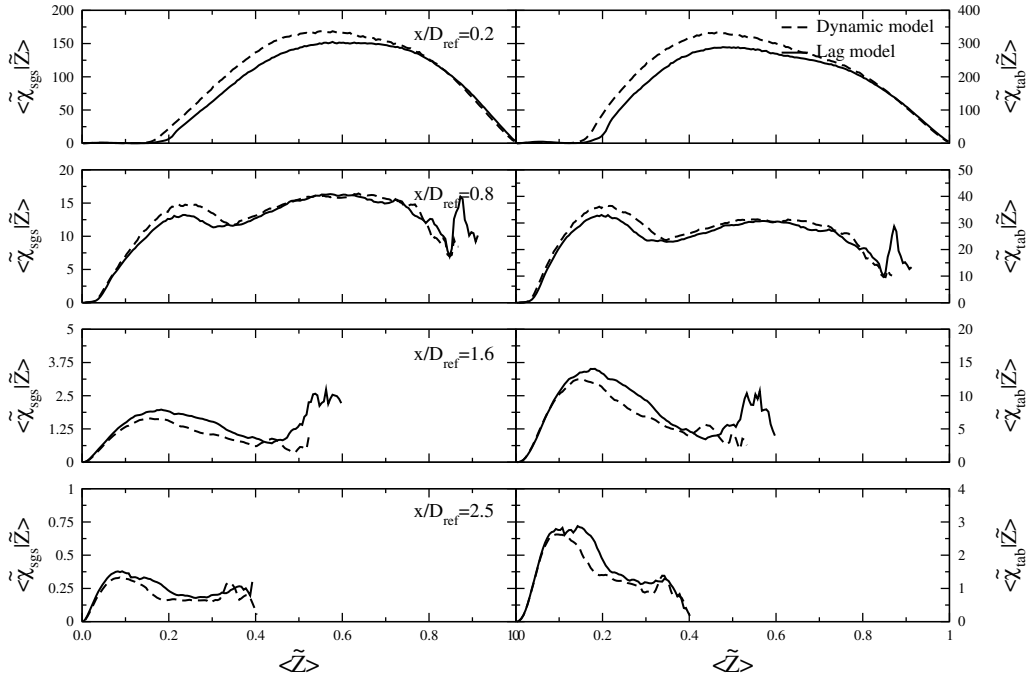


FIGURE 8. Mean values of  $\chi_s$  and  $\theta$  conditioned on the mixture fraction, at four downstream locations,  $x/D_{ref} = 0.2, 0.8, 1.6, 2.5$  (from top to bottom).

variance. We expect the lag effect to be important in applications with high sensitivity to the dissipation terms, such as non-premixed combustion. Also, this approach might prove beneficial for applications where the flow timescales are significantly faster than the turbulence timescales, such as scramjet combustion.

The immediate future work includes a posteriori testing of the lag-models in more idealized environment where the model effects can be clearly isolated. Such tests would not only provide a better assessment of whether the lag-modeling approach has inherent advantages over existing approaches, but also would (hopefully) identify specifically in what situations the lag itself is important.

Although the lag-modeling approach to the dissipation terms appears to improve the results for the regions of high sensitivity to the dissipation terms, we must empathize that the overall quality of the lag-model is highly dependent on the quality of the source terms in the lag-equations,  $\Pi$  and  $\Lambda$ . These terms, in turn, directly depend on the quality of the models for  $\tau_{ij}$  and  $h_i$ . This brings attention to the structural models for these quantities, as opposed to the functional models (as classified by Sagaut 2006). The former try to predict the actual configuration of  $\tau_{ij}$  and  $h_i$ , which appears crucial for good prediction of the local energy transfer and variance source, which in turn affects the performance of the lag-models.

## Acknowledgments

Numerical simulations were performed on WCR and JHF clusters at Center for Turbulence Research and on Coyote cluster at Los Alamos National Laboratory. Support

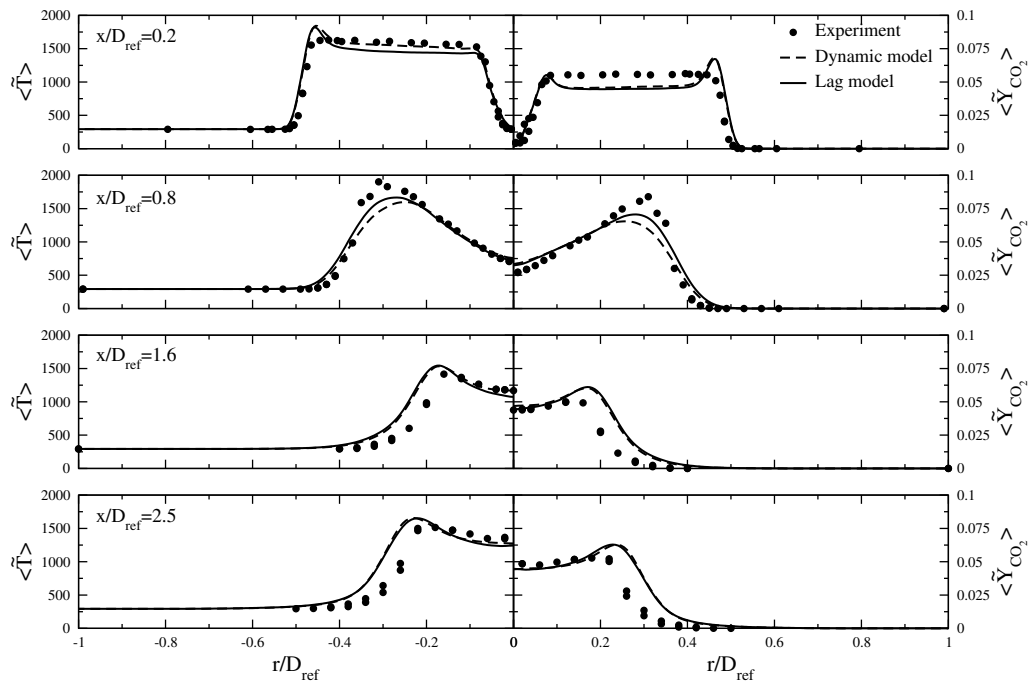


FIGURE 9. Statistics of the mean of temperature and the mean of  $\text{CO}_2$  mass fraction at four downstream locations, namely  $x/D_{ref} = 0.2, 0.8, 1.6, 2.5$  (from top to bottom). The experiment is represented by full circles, the simulation based on a standard dynamic procedure to evaluate the subgrid scalar dissipation rate is shown by the dashed line, and the simulation based on the lag-model corresponds to the solid line.

from NASA under grants NNX07AC72A-4 (S.C.) and NNX08AB30A (J.L.) is gratefully acknowledged.

#### REFERENCES

- AL-ABDELI, Y. A. & MASRI, A. R. 2003 Stability characteristics and flow fields of turbulent non-premixed swirling flames. *Comb. Theory Modelling* **7**, 731–766.
- BALARAC, G., PITSCHE, H. & RAMAN, V. 2008a Development of a dynamic model for the subfilter scalar variance using the concept of optimal estimators. *Phys. Fluids* **20** (3), 035114.
- BALARAC, G., PITSCHE, H. & RAMAN, V. 2008b Modeling of the subfilter scalar dissipation rate using the concept of optimal estimators. *Phys. Fluids* **20** (9), 091701.
- BOWMAN, T. C., HANSON, R. K., DAVIDSON, F. D., GARDINER, W. C., LISSIANSKI, V., SMITH, G. P., GOLDEN, D. M., FRENKLACH, M. & GOLDENBERG, M. 1997 Gri-mech 2.11. <http://www.me.berkeley.edu/gri-mech/>.
- CHUMAKOV, S. G. 2007 Scaling properties of subgrid-scale energy dissipation. *Phys. Fluids* **19**, 058104.
- CHUMAKOV, S. G. & RUTLAND, C. J. 2004 Dynamic structure models for scalar flux and dissipation in large eddy simulation. *AIAA J.* **42** (6), 1132–1139.
- CHUMAKOV, S. G. & RUTLAND, C. J. 2005 Dynamic structure subgrid-scale models for large eddy simulation. *Int. J. Numer. Meth. Fluids* **47**, 911–923.

- COOK, A. W. & BUSHE, W. K. 1999 A subgrid-scale model for the scalar dissipation rate in nonpremixed combustion. *Phys. Fluids* **11** (3), 746 – 8.
- DESJARDINS, O., BLANQUART, G., BALARAC, G. & PITSCH, H. 2008 High order conservative finite difference scheme for variable density low Mach number turbulent flows. *J. Comput. Phys* **227**, 7125–7159.
- GHOSAL, S. 1999 Mathematical and physical constraints on Large-Eddy simulation of turbulence. *AIAA J.* **37** (4), 425–433.
- GHOSAL, S., LUND, T. S., MOIN, P. & AKSELVOLL, K. 1995 A dynamic localization model for large-eddy simulation of turbulent flows. *J. Fluid Mech.* **319**, 353–385.
- JIMÉNEZ, C., DUCROS, F., CUENOT, B. & BÉDAT, B. 2001 Subgrid scale variance and dissipation of a scalar field in large eddy simulations. *Phys. Fluids* **13** (6), 1748–1754.
- KALT, P. A. M., AL-ABDELI, Y. A., MASRI, A. R. & BARLOW, R. S. 2002 Swirling turbulent non-premixed flames of methane: Flow field and compositional structure. *Proc. Combust. Inst.* **29**, 1913–1919.
- KAUL, C. M., RAMAN, V., BALARAC, G. & PITSCH, H. 2009 Numerical errors in the computation of subfilter scalar variance in large eddy simulations. *Phys. Fluids* **21** (5), 055102.
- MASRI, A. R. 2006 Web site for the Sydney swirl flame series. <http://www.aeromech.usyd.edu.au/thermofluids>.
- MASRI, A. R., KALT, P. A. M. & BARLOW, R. S. 2004 The compositional structure of swirl-stabilised turbulent nonpremixed flames. *Combust. Flame* **137**, 1–37.
- MENEVEAU, C., LUND, T. S. & CABOT, W. H. 1996 A Lagrangian dynamic subgrid-scale model of turbulence. *J. Fluid Mech.* **319**, 353–385.
- PETERS, N. 1983 Local quenching due to flame stretch and non-premixed turbulent combustion. *Combust. Sci. Tech.* **30**, 1–17.
- PETERS, N. 1984 Laminar diffusion flamelet models in non-premixed turbulent combustion. *Prog. Energy Combust. Sci.* **10** (3), 319–339.
- PIERCE, C. D. & MOIN, P. 1998 A dynamic model for subgrid-scale variance and dissipation rate of a conserved scalar. *Phys. Fluids* **10** (12), 3041–3044.
- PITSCH, H. 2006 Large-eddy simulation of turbulent combustion. *Annu. Rev. Fluid Mech* **38**, 453–82.
- SAGAUT, P. 2006 *Large Eddy Simulation for Incompressible Flows: An Introduction*. Springer-Verlag.
- SCHUMANN, U. 1975 Subgrid scale model for finite difference simulations of turbulent flows in plane channels and annuli. *J. Comput. Phys.* **18** (4), 376 – 404.
- YOSHIZAWA, A. & HORIUTI, K. 1985 A statistically-derived subgrid-scale kinetic energy model for the Large-Eddy simulations of turbulent flows. *J. Phys. Soc. Jpn.* **54** (8), 2834 – 2839.